



OPEN ACCESS

EDITED BY
Venkatramanan Senapathi,
Alagappa University, India

REVIEWED BY
Hadi Shafai Moghadam,
Damghan University, Iran
Mustafa Açlan,
Yüzüncü Yıl University, Turkey

*CORRESPONDENCE
Vikas Adlakha,
vikas.himg@gmail.com

SPECIALTY SECTION
This article was submitted to Structural
Geology and Tectonics,
a section of the journal
Frontiers in Earth Science

RECEIVED 25 August 2022
ACCEPTED 28 November 2022
PUBLISHED 08 December 2022

CITATION
Pundir S, Adlakha V, Kumar S, Singhal S
and Das S (2022), A newly identified
cryogenian (ca. 806 ma) basement
tonalite gneiss from the Eastern
Karakoram, NW India: Constraints from
geochemistry and zircon U-
Pb geochronology.
Front. Earth Sci. 10:1027801.
doi: 10.3389/feart.2022.1027801

COPYRIGHT
© 2022 Pundir, Adlakha, Kumar, Singhal
and Das. This is an open-access article
distributed under the terms of the
[Creative Commons Attribution License
\(CC BY\)](https://creativecommons.org/licenses/by/4.0/). The use, distribution or
reproduction in other forums is
permitted, provided the original
author(s) and the copyright owner(s) are
credited and that the original
publication in this journal is cited, in
accordance with accepted academic
practice. No use, distribution or
reproduction is permitted which does
not comply with these terms.

A newly identified cryogenian (ca. 806 ma) basement tonalite gneiss from the Eastern Karakoram, NW India: Constraints from geochemistry and zircon U-Pb geochronology

Shailendra Pundir¹, Vikas Adlakha^{1*}, Santosh Kumar²,
Saurabh Singhal¹ and Satyabrata Das¹

¹Wadia Institute of Himalayan Geology, Dehradun, Uttarakhand, India, ²Department of Geology, Centre of Advanced Study, Kumaun University, Nainital, Uttarakhand, India

The Karakoram Terrane (KT) represents the southern margin of the Eurasian Plate, mainly consisting of Late Jurassic-Early Cretaceous subduction-related granites and post-collisional Miocene leucogranites, which intrude the Late Neo-Proterozoic basement. We report for the first time the existence of the Cryogenian KT basement as recorded from the geochemistry and geochronology of tonalite gneiss (ca. 806 Ma) in the southeastern Karakoram terrane, NW India. Geochemically, the studied tonalite gneiss is slightly peraluminous (Molar $Al_2O_3/CaO+Na_2O+K_2O=1.1$), calc-alkaline volcanic-arc granitoid, strongly fractionated REE ($La_N/Yb_N=33.99$), and high $Sr/Y=19.75$, more akin to its affinity with Tonalite-trondhjemite-granodiorite (TTG)/adakite. The whole-rock elemental data suggest that tonalite gneiss is more likely sourced from ancient mafic lower crust where garnet remained in the residue. The petrogenetic modeling of REE suggests that the melt similar to the observed tonalite gneiss can be generated through ~50% partial melting of a mafic lower crust with garnet, clinopyroxene, and amphibole assemblage. The synthesis and comparison of present and published Proterozoic magmatic records on the rocks from KT strongly dictate that the produced partial melt similar to observed tonalite gneiss most likely served as the parental melt for the development of TTGs in the Southern Pamir and more evolved granitoid in the Central Tibetan terrane. We propose that the studied tonalite gneiss from the southeast Karakoram is a product of Neoproterozoic Andean-type orogeny formed on the northwestern margin of the Rodinia supercontinent. Thus, our study favors the first time, the position of KT within the Cimmerian belt along with other East Asian continental blocks.

KEYWORDS

cryogenian magmatism, geochronology, geodynamics, karakoram, trans-himalaya

1 Introduction

The supercontinent Rodinia is considered to have assembled during Mesoproterozoic to Neoproterozoic (~1300 to 900 Ma), which fragmented later during late Neoproterozoic (Meert and Torsvik, 2003; Li et al., 2008; Cawood et al., 2016). The timing and origin of spatially distributed felsic magmatic rocks of Neoproterozoic time from the Asian terranes provide evidence on the assembly, growth and break-up of the Rodinia supercontinent (e.g., Zhao et al., 2018). Various studies on the paleogeographic reconstruction of Pamir, Tarim, Qiangtang, and Lhasa Terranes from East-Asia suggest the location of these continental blocks on the northwestern margin of the Rodinia supercontinent (eg., Condie, 2001; Li et al., 2008; Dong et al., 2011; Cawood et al., 2013; Cawood et al., 2016; Merdith et al., 2017; Zhao et al., 2018; Hu et al., 2018a; Hu et al., 2018b; Zhou et al., 2019; Kang et al., 2019). Later, these East Asian terranes formed the part of Gondwanaland during the Paleozoic hence all belong to Gondwanan ancestry (Crawford, 1974; Şengör 1984; Yeh and Shellnutt, 2016). The Karakoram Terrane (KT), southern Pamir, Tarim, Qiangtang, and Lhasa broke from the Gondwanan margin in the Early Permian and moved in the north which then collided with Eurasian margin in Middle Triassic that formed the Cimmerian orogen (Yeh and Shellnutt, 2016).

The KT represents the southern margin of the Eurasian Plate and is considered geologically equivalent to the southeast and central Pamir Terranes in the west and Qiangtang Terrane in the east (Figure 1A; Robinson, 2015; Villarreal et al., 2020). Geologically, the KT mainly consists of the Late-Jurassic to Early Cretaceous Karakoram Batholith (KB) which mainly consist of pre-collisional calc-alkaline I-type granitoids as the main magmatic event that formed due to subduction of Neo-Tethys oceanic lithosphere beneath south Eurasian plate margin (e.g., Fraser et al., 2001; Heuberger et al., 2007; Jain and Singh, 2009; Boutonnet et al., 2012; Phillips et al., 2013; Sen et al., 2014; Pundir et al., 2020a; Pundir et al., 2020b), and the Early Cretaceous to Late-Miocene Karakoram Metamorphic complex which mainly consists of regional Barrovian facies kyanite- and sillimanite-grade metamorphic rocks and leucogranites (e.g., Fraser et al., 2001; Rolland et al., 2009; Streule et al., 2009; Wallis et al., 2014). Similar to the KT, the southern Pamir records Late Jurassic-Late Cretaceous calc-alkaline subduction related I-type granitoids (Liu et al., 2020 and references therein) and Qiangtang terrane from central Tibet records Late Triassic to Late Cretaceous subduction-related I-type granites (e.g., Kapp et al., 2003; Peng et al., 2015; He et al., 2019). The Late Neo-Proterozoic terrane granitoids along the southern margin of the Eurasian Plate is exposed sporadically (e.g., the western Karakoram, the southeast Pamir, and the southern Qiangtang and Northern Lhasa region (central Tibet)) (Rolland et al., 2002; Dan et al.,

2020; Liu et al., 2020). In the KT the record of crystalline Late Neo-Proterozoic basement occurs only in a few regions of the western Karakoram where the metadiorite (ca. 651 Ma; $^{40}\text{Ar}/^{39}\text{Ar}$) outcrops to the north of the Shyok Suture zone (SSZ) (Rolland et al., 2002). A record of pre-Ordovician granitic intrusion to the north of the Karakoram Batholith is also reported (Fort et al., 1994). However, no shreds of evidence on Late Neo-Proterozoic crystalline basement rocks are available from southeastern KT, India, unlike the Lhasa, Qiangtang, southeast Pamir, and western KT. Thus, the non-availability of such Late Neo-Proterozoic magmatism records in SE Karakoram limits our understanding of Late Neo-Proterozoic evolution and Paleogeographic reconstruction of the Karakoram and western Tibet. The geological, geographical, and geochronological correlation of the KT to the Pamir range to the NW, and central Tibet to the SE is important to understand the origin and position of the KT in the Cimmerian belt (e.g., Afghanistan, Pamir, Tarim, Qiangtang, and Lhasa terranes) that formed the northern margin of the Gondwanaland during the Paleozoic (e.g., Şengör, 1984).

This study presents the first whole-rock geochemical and zircon U-Pb geochronology of a sample of Neo-Proterozoic granite gneiss from the KT. We analyze the present set of new data in combination with the published geochemical record on similar Neoproterozoic granites of the Pamir Terrane and central Tibet to constrain the petrogenesis of the KT basement during the Neoproterozoic supercontinent cycle. Our study provides significant evidence to reveal the Paleogeography of the SE Karakoram in the context of Rodinia and Cimmerian terrane, which existed in the geological past.

2 Regional geology

The India-Asia collision zone or Trans-Himalaya and KT litho-tectonic units represent the southern margin of the Eurasian Plate (e.g., Searle et al., 1998; Jain and Singh, 2008; Searle and Hacker, 2019). The KT lies to the northwest of the Himalayan Mountains and extends from the Afghan block in the west to southwest Tibet in the east (Figure 1). The Rushan-Pshart Suture zone forms the northern boundary of the KT, where it abuts against the southern Pamir mountains, and the Shyok Suture Zone (SSZ) forms its southern boundary, which separates it from the Ladakh Batholith (Figure 1A; e.g., Schwab et al., 2004; Searle and Hacker, 2019).

The study area forms the part of NW India where the KT can be divided into three main geological units, namely 1) Karakoram Fault (KF) zone, 2) Karakoram Metamorphic Complex (KMC), and 3) Karakoram Batholith (KB) (e.g., Jain and Singh, 2008) (Figure 1B).

The southern margin of KT bounds the ~1000 km long lithospheric scale dextral strike-slip KF to the south (Searle

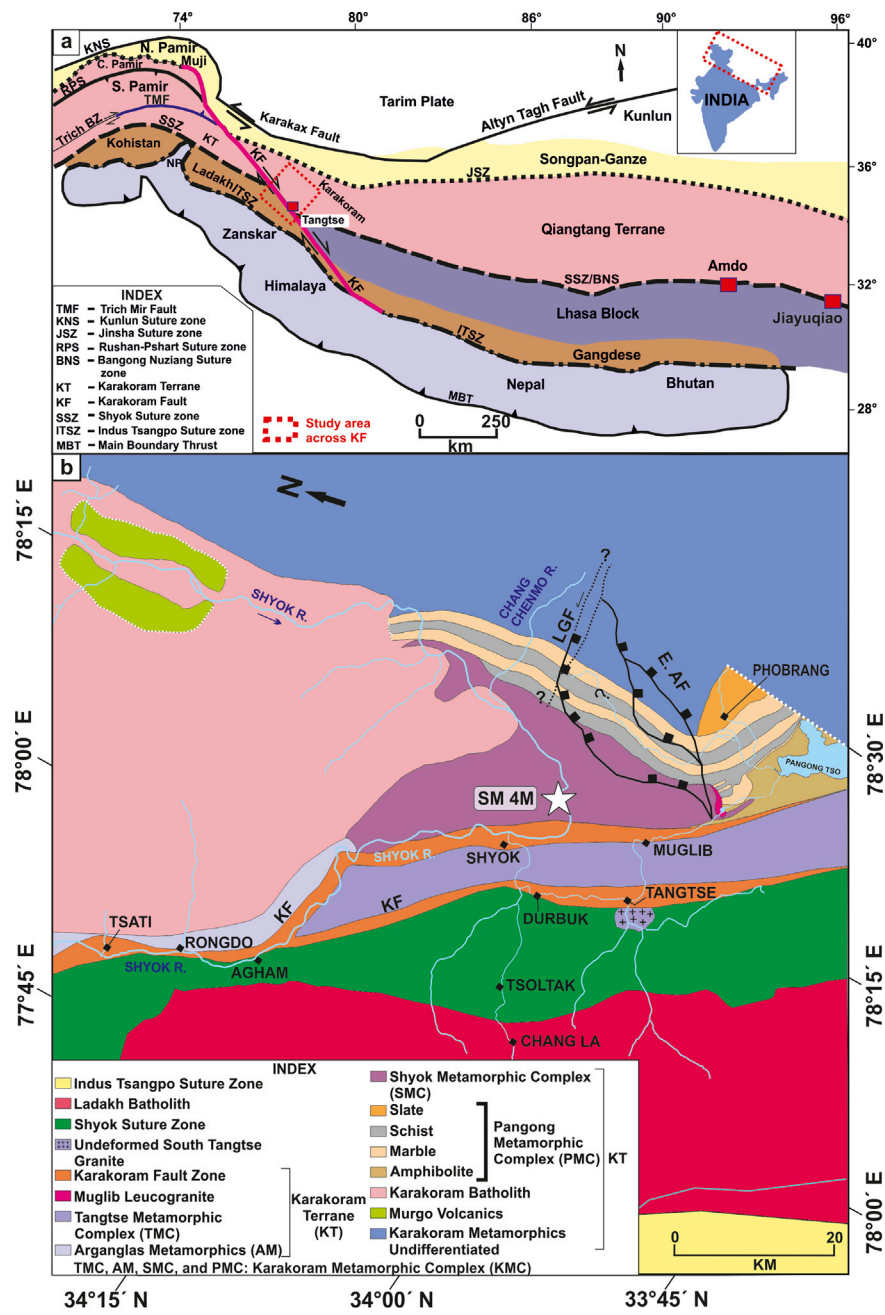


FIGURE 1
 (A) Map showing the main tectonic structures and sutures in the Himalaya and Tibet (modified after Searle, 2011). The red dashed rectangle indicates the map area in Figure 1B. (B) Geological map of the study region (modified after Jain 2014; Pundir et al., 2020a). LGF: Longmu-Ghoza Co fault; E. AF: East Angmong Fault.

et al., 1998) (Figure 1A). In the SE Karakoram, the KF splays into two strands named the Tangtse strand in the SW and the Muglib strand in the NE, which forms a zone consisting of mylonite, granite gneiss, amphibolites, and leucogranites (e.g., Srimal, 1986; Searle et al., 1998; Weinberg and Mark, 2008). Locally,

this zone is known as Tangtse Metamorphic Complex (TMC) or Pangong Injection Complex (PIC), and in the NW of Muglib strand, it is known as Shyok Metamorphic Complex (SMC) (Figure 1B; Searle et al., 1998; Pundir et al., 2020a). An undeformed porphyritic granite body of KB is exposed to the

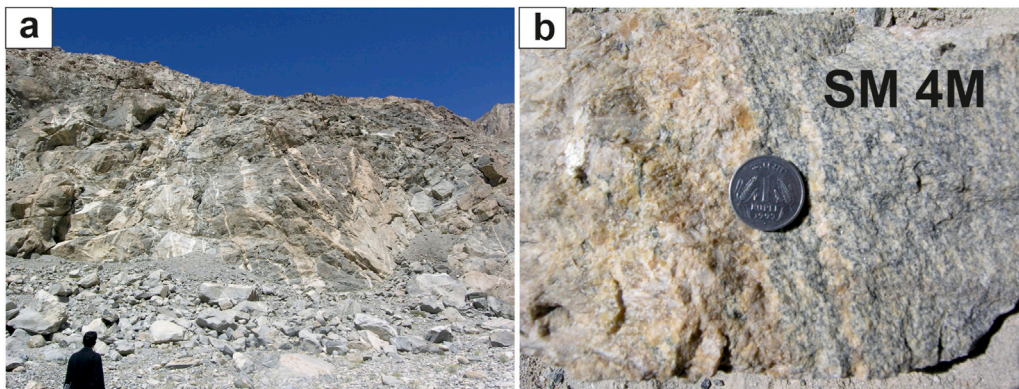


FIGURE 2
 (A) High-grade metamorphic rocks and zone of partial melting observed to the north of the Shyok-Muglib strand of the KF known as SMC. (B) Collected sample of tonalite gneiss SM 4 M from the SMC zone of KB.

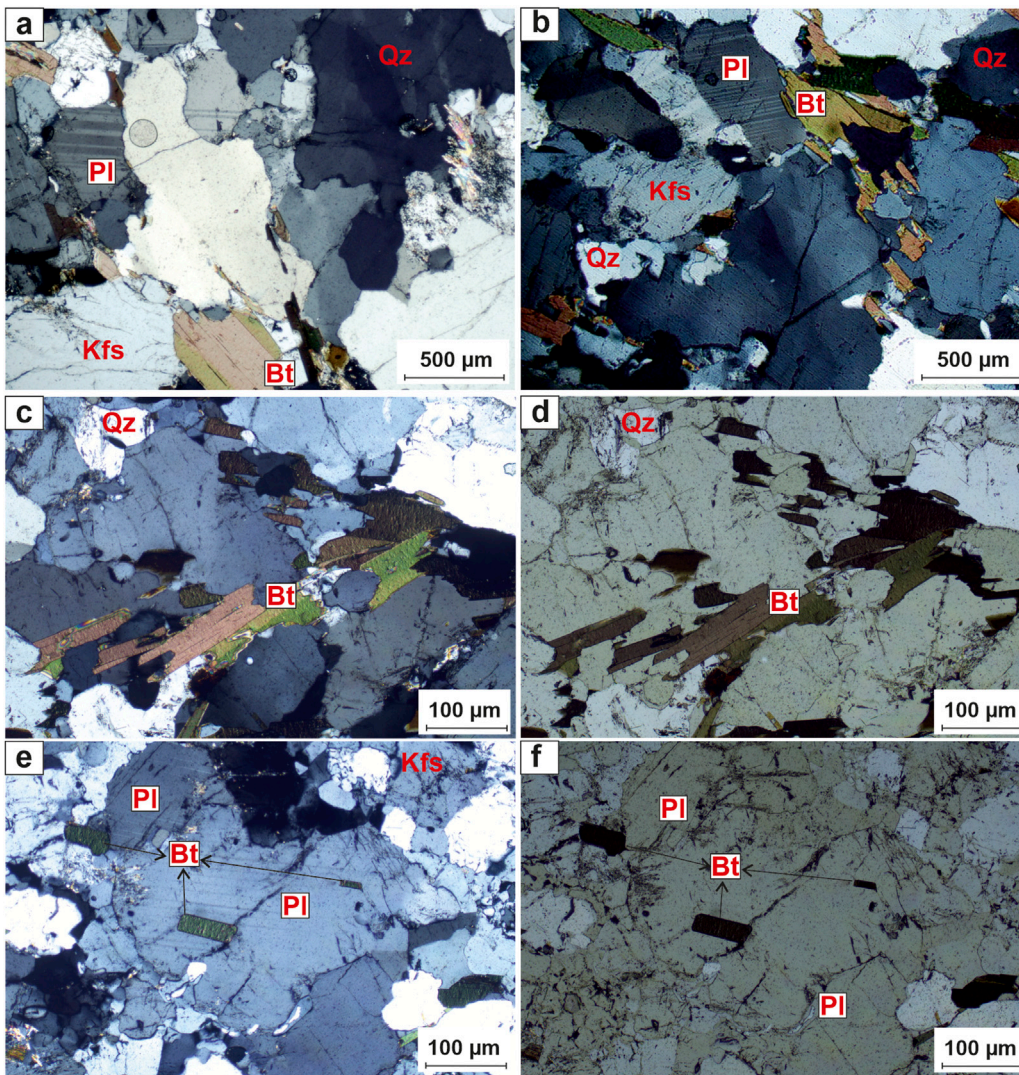
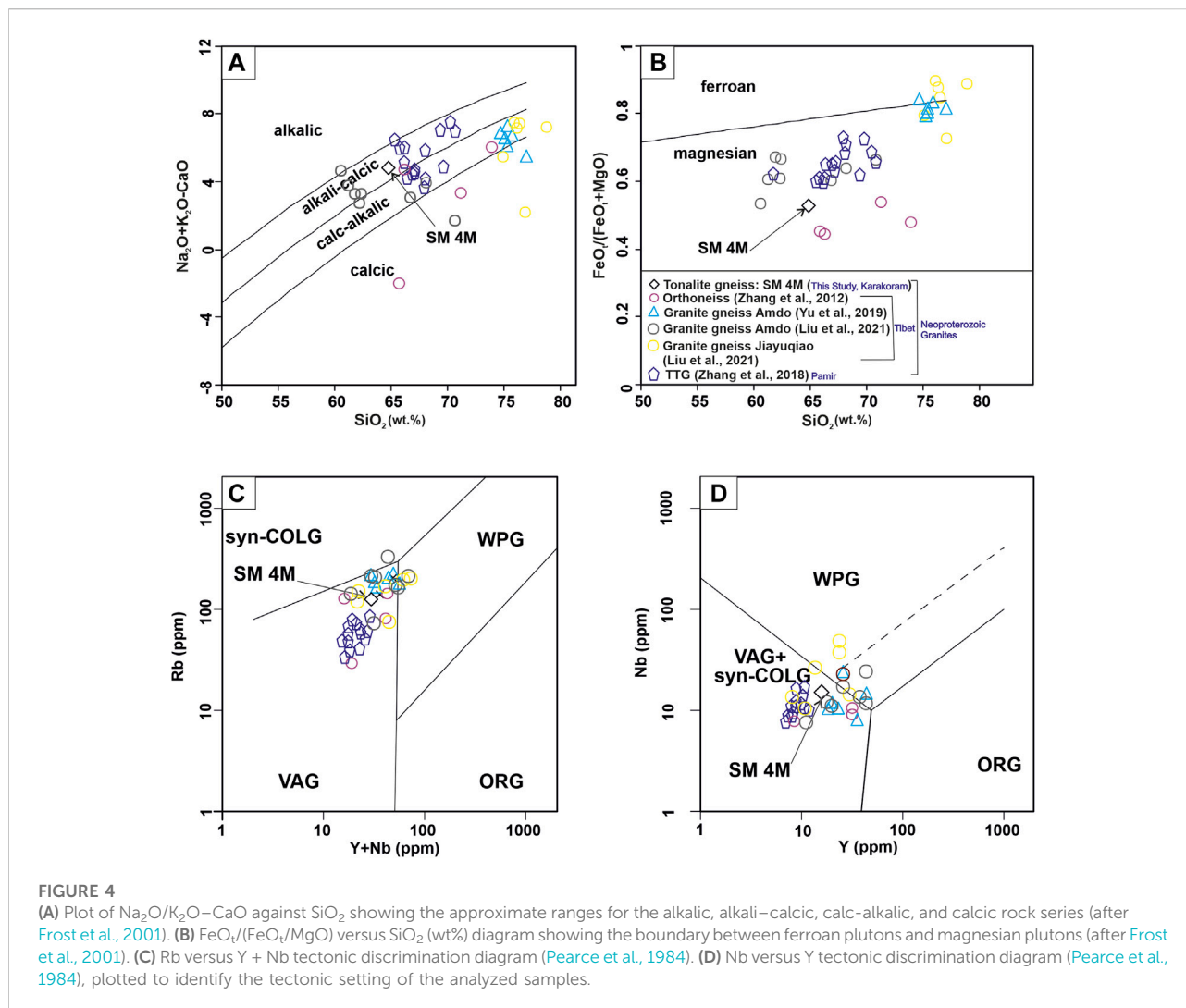


FIGURE 3
 (A–F) Microphotograph of the tonalite gneiss SM 4 M mainly consists of quartz (Qz), K-feldspar (Kfs), plagioclase (Pl), and biotite (Bt).



north of KMC (Pundir et al., 2020a; Pundir et al., 2020b). The KB is mainly composed of hornblende-biotite and biotite bearing subduction-related magmatic rock suites, which are considered to be emplaced prior to the India-Asia collision (e.g., Jain and Singh, 2008), which later suffered submagmatic to solid state ductile deformation during Late-Cretaceous (Bose et al., 2022). The granites are porphyritic, consisting of randomly oriented ~2–5 cm long plagioclase and K-feldspar phenocrysts embedded in a fine-grained felsic groundmass (Pundir et al., 2020a). However, the TMC/PIC and SMC mainly consists of mylonite granite, foliation-parallel leucosome, i.e., deformed leucogranite as well as undeformed leucogranites, granite gneisses, amphibolites, bt-sammites and calc-silicate rocks (e.g., Reichardt et al., 2010; Boutonnet et al., 2012; Pundir et al., 2020a; Pundir et al., 2020b). In this study, the granite gneiss is exposed in the SMC (Figures 2A,B). This is biotite plagioclase bearing granitoid and is found in association with subduction-related Late-Jurassic Early- Cretaceous granitoids.

3 Sample selection and analytical methods

The sample of granite gneiss (SM 4 M) was collected from the SMC of the KT zone (Location: N 34.151128°; E 78.225104°) (Figure 1A and Figures 2A,B) and treated for whole-rock major and trace element analyses, and zircon U-Pb geochronology.

The whole-rock major and trace element compositions were analyzed using a wavelength dispersive X-Ray Fluorescence (Bruker Tiger S-8) on pressed-powder pellets at Wadia Institute of Himalayan Geology (WIHG), Dehradun, India. XRF technique analytical precision for both major and trace elements lie within $\pm 2\%$ – 3% and $\pm 5\%$ – 6% , respectively (Saini et al., 2007; Khanna, 2009). The rare Earth elements (REEs) were determined from the digested solution of rock powder using a Perkin-Elmer SCIEX-ICP Mass Spectrometer model ELAN-DRC-e. Rock standards (JG-2, GH, and MB-H) were used for calibration. The

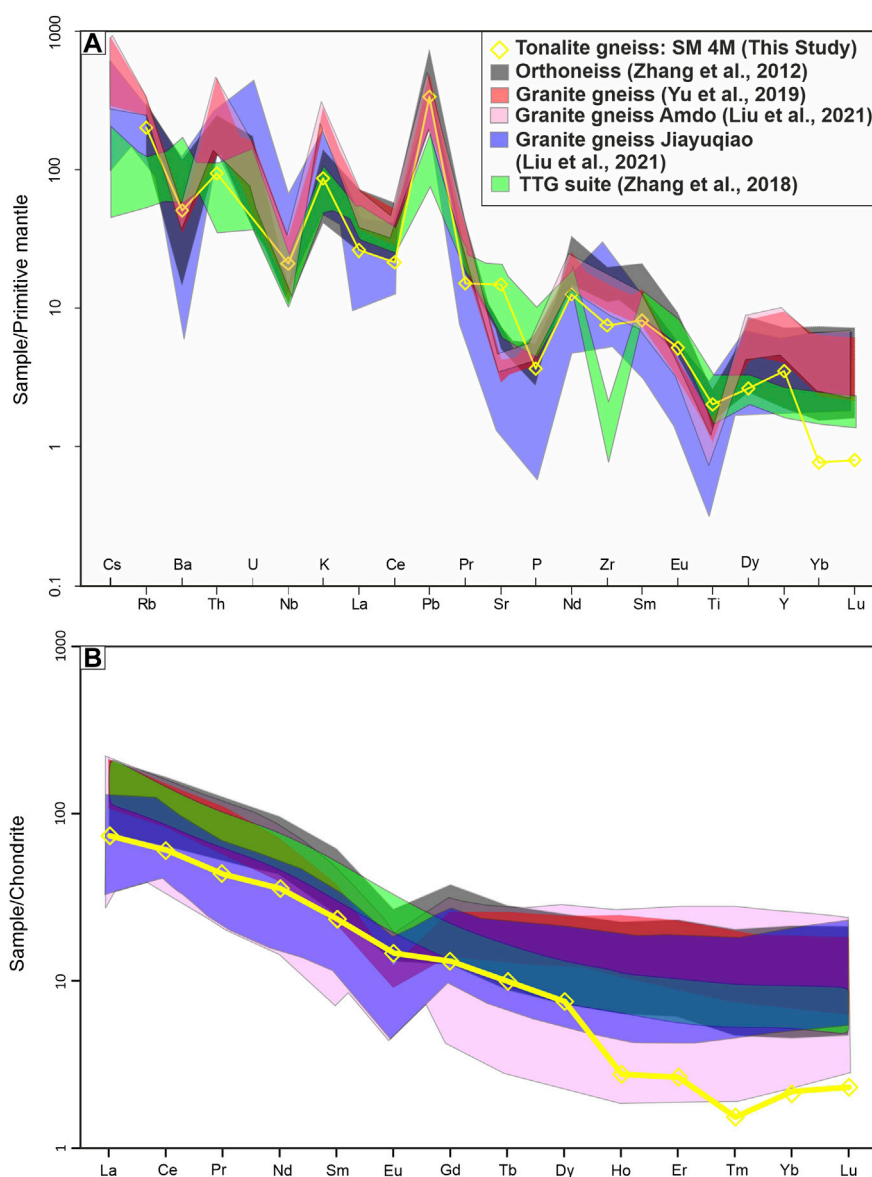


FIGURE 5

(A) Primitive mantle normalized spider diagram (after Sun and McDonough, 1989). (B) Chondrite-normalized REE patterns (after Sun and McDonough, 1989).

geochemical data processing and plotting were done using Geochemical Data Toolkit software (GCDkit, Janoušek et al., 2006).

Zircon U–Pb dating was performed using LA-MC-ICPMS (Neptune-plus, ThermoFisher Scientific Inc) fitted with a 193 nm excimer laser (UV Laser, Model Analyte G2, Cetec-Photon machine Inc.), equipped with high-performance HelEx-II sample chamber installed at WIHG, Dehradun. About 4 kg of the sample was crushed, powdered, and processed for zircon separation using jaw crusher, disk mill, gravity separation using Holman-Wilfley shaking table, magnetic separation using magnetic barrier separator, and heavy liquids separation using Bromoform (CHBr_3) and

Diiodomethane (CH_2I_2). Euhedral to subhedral zircon grains were hand-picked up using a stereo zoom microscope, and zircons were mounted using PFA Teflon film at a temperature of $\sim 275^\circ\text{C}$. The internal zircon surfaces were exposed by means of 2400 grit sandpaper, and polished by 1- and 0.25-micron diamond paste. The zircon mounts were gold-coated for cathodoluminescence (CL) imaging using a Gatan Chroma CL UV attached to a Carl-Zeiss EVO 40 EP scanning electron microscope. The probe current varies from 10 to 20 nA. A zircon spot diameter of 20 μm was preferred to carry out U–Pb *in-situ* analysis. The standard 91500 zircon [(TIMS normalization

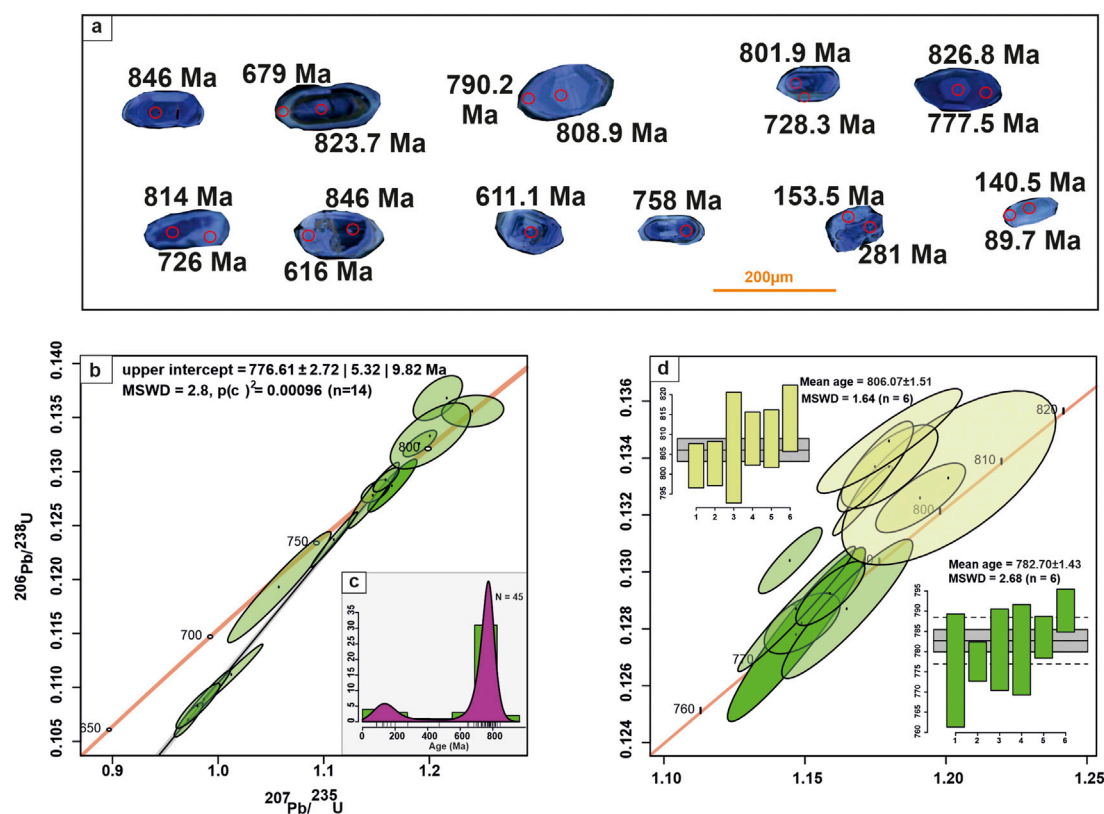


FIGURE 6

(A) Representative CL images of the studied tonalite gneiss, (B) ^{206}Pb – ^{238}U ages and Concordia diagrams for LA-MC-ICP-MS zircon data plots, (C) Kernel density plot showing the distribution of ^{206}Pb – ^{238}U ages. (D) Weighted mean ages for the most concordant ^{206}Pb – ^{238}U ages.

data $^{206}\text{Pb}/^{238}\text{U} = 1062.32 \pm 2.22$ Ma; 2 sigma) (Wiedenbeck et al., 1995) and Plešovice zircon standard ID TIMS $^{206}\text{Pb}/^{238}\text{U}$ age = 337.13 ± 0.37 Ma (Sláma et al., 2008)] were used for correction of U-Pb downhole fractionation, accuracy assessment and data reduction (Paton et al., 2011), for detailed methodology see Mukherjee et al., 2017. Isoplot R was used for processing and plotting the U-Pb isotopic data (Vermeesch, 2018).

4 Petrography

The granite gneiss (SM 4 M) is a medium to coarse-grained rock mainly consisting of quartz (Qz), plagioclase (Pl), K-feldspar (Kfs), biotite (Bt), zircon (Zrn), and apatite (Ap) (mineral's symbols after Whitney and Evans, 2010) (Figure 3). Biotite is the only ferromagnesian phase present in the sample which are subhedral to euhedral mainly consisting of one set of basal cleavage showing its primary nature (Figures 3A–F). The quartz is showing slight undulose extinction and is devoid of any sub-solidus deformation e.g., sub-grain rotation and grain boundary migration. Plagioclase crystals are subhedral to euhedral and display polysynthetic twinning (Figures 3B,C).

The K-feldspar is present in the form of orthoclase. As per the International Union of Geological Sciences (IUGS) recommended modal Q-A-P parameters (Supplementary Figure S1; Streckeisen 1976; Le Maitre 2002), the granite gneiss (SM 4 M) corresponds to tonalite.

5 Results

5.1 Whole-rock geochemistry, and zircon U–Pb geochronology results of the tonalite gneiss (SM 4 M)

Whole-rock major and trace-element geochemical data for the tonalite gneiss is given in Supplementary Table S1. The SiO_2 content of the tonalite gneiss is 64.85 wt% with 2.63 wt% K_2O and 4.65 wt% Na_2O . Molar A/CNK [$[\text{Al}_2\text{O}_3]/(\text{CaO}+\text{Na}_2\text{O}+\text{K}_2\text{O}=1.1)$] ratio suggests a slightly peraluminous nature of the tonalite gneiss (Supplementary Table S1). The tonalite gneiss is alkali-calcic and magnesian in nature and belongs to the subduction-related volcanic arc granitoid (VAG), and VAG+syn-collisional granitoid (syn-COLG) fields (Figures 4A–D). The tonalite gneiss shows negative

TABLE 1 U-Pb LA-MC-ICPMS isotopic data of analyzed tonalite gneiss from Karakoram Terrane, NW India.

Spot	U (ppm)	Th (ppm)	Th/U	²⁰⁷ Pb/ ²³⁵ U	±%	²⁰⁶ Pb/ ²³⁸ U	±%	²⁰⁷ Pb/ ²³⁵ U (Ma)	±Ma	²⁰⁶ Pb/ ²³⁸ U (Ma)	±Ma
SM 4 M (tonalite gneiss)											
1_C	284	335	1.18	1.25	0.02	0.140	0.003	823	11	846	15
1_R	304	161.1	0.53	0.90	0.02	0.100	0.002	651.6	9.9	616	12
2_C	375	84.9	0.23	0.38	0.03	0.045	0.003	327	21	281	20
2_R	406	12.2	0.03	0.16	0.00	0.024	0.001	152.8	3.6	153.5	3.8
2_C	197	164	0.83	0.92	0.02	0.104	0.002	663.5	8.1	637	10
3_C	475	325	0.68	0.88	0.01	0.099	0.001	641	4.5	611.1	5
4_C	298	325	1.09	1.11	0.01	0.125	0.001	757.8	4.9	758	6.9
5_C	201	115	0.57	0.66	0.05	0.067	0.005	507	28	416	30
5_CR	172	133	0.77	1.30	0.02	0.140	0.002	846.9	9.8	846	13
5_CR2	169.6	157	0.93	1.15	0.02	0.128	0.003	775.5	9.7	775	14
6_C1	47.4	34.5	0.73	1.15	0.01	0.128	0.001	776.8	5.1	777.5	5
6_C2	39.9	32.5	0.81	1.21	0.02	0.137	0.002	804.2	8.8	826.8	9.5
6_CR	40.8	25.1	0.62	1.18	0.01	0.134	0.001	791.2	6.5	808.8	6.6
7_C	296	288	0.97	1.20	0.03	0.133	0.003	805	13	806	14
8_C	120.5	135.6	1.13	1.18	0.01	0.134	0.001	788.7	5.3	808.9	7.2
8_CR	164.9	169.1	1.03	1.14	0.01	0.130	0.001	774.7	4.4	790.2	5.4
9_C	430	350	0.81	1.17	0.01	0.133	0.001	786.7	4	801.9	5.9
9_R	313	344	1.10	1.06	0.01	0.120	0.001	731.6	3.2	728.3	4.6
10_C1	117.6	64.7	0.55	1.06	0.04	0.119	0.004	730	20	726	24
10_C2	107.6	58.2	0.54	1.18	0.02	0.135	0.002	791.1	9.9	814	8.7
11_R1	620	2.44	0.00	0.09	0.00	0.014	0.000	88.1	2.6	89.7	2.6
11_C2	352	15	0.04	0.16	0.01	0.022	0.001	149.8	4.7	140.5	4.1
11_R2	524	3.11	0.01	0.09	0.00	0.014	0.000	86.49	0.96	87.52	0.65
12_C	628	760	1.21	0.88	0.01	0.097	0.002	641.5	7.2	595.9	9.8
12_R	466	38.43	0.08	0.13	0.00	0.019	0.000	125.2	2.3	123.6	1.9
13_R	224	63.5	0.28	0.44	0.01	0.049	0.002	370	11	306.7	9.5
13_C	186.3	150	0.81	1.19	0.01	0.133	0.001	796.1	6.2	802.6	5.7
14_C1	181	110	0.61	1.03	0.05	0.116	0.005	717	23	705	30
14_C2	200	152	0.76	1.15	0.02	0.129	0.002	775.4	8	780	10
15_C	353	381	1.08	1.04	0.01	0.117	0.001	724.7	4.4	712.2	5.3
15_R	109.7	41.25	0.38	0.98	0.02	0.108	0.002	694.1	8.8	662.7	9.8
16_C1	284	236	0.83	1.11	0.02	0.124	0.002	759.3	9	752	12
16C2	49	28.2	0.58	1.24	0.02	0.136	0.001	819	10	819.4	6.9
17_C	234.4	230.1	0.98	1.06	0.01	0.116	0.001	733.2	6.4	709.2	7.8
17_R	314.1	29.2	0.09	0.19	0.00	0.028	0.000	176.3	2.8	175.6	2.1
18_C	76.8	72.4	0.94	1.09	0.02	0.116	0.002	746	9.6	707	10
18_C2	172	46.1	0.27	1.13	0.02	0.121	0.002	769.4	7.1	738	9.2
19_C	142	54.4	0.38	1.27	0.02	0.136	0.002	830.3	8.6	823.7	9.7
19_R	233	79.5	0.34	1.01	0.02	0.111	0.002	710	12	679	13
20_C	262	213	0.81	1.17	0.02	0.129	0.002	783.8	8.8	781	11
20_C2	123.3	110.2	0.89	1.16	0.01	0.129	0.001	781.6	4.7	783.5	5.3
21_C	228	158.7	0.70	0.99	0.02	0.109	0.002	698	11	666	13
21_C2	263	154	0.59	1.13	0.02	0.118	0.001	767	11	716.7	6.6
22_C	196.8	152.5	0.77	0.83	0.01	0.094	0.002	616.8	7.1	579	9.1
22_C2	206.7	174	0.84	0.97	0.01	0.107	0.001	689.2	5.6	655.2	7.6

anomalies for Nb and Ti (Figure 5A), along with light REEs (LREEs) enrichment relative to heavy REEs (HREEs) ($La_N/Yb_N = 33.99$; $Ce_N/Yb_N = 27.76$) (Figure 5B).

Zircon grains from tonalite gneiss are long prismatic and euhedral to subhedral in shape (Figure 6A). The CL images shows the oscillatory growth zoning in the cores while the rims are mostly homogeneous in nature (Figure 6A). Forty-five spot analyses were carried out on 22 zircon grains. Rims with Late Jurassic–Early Cretaceous have low Th/U values of 0.004–0.093, typical of metamorphic origin (e.g., Rubatto 2002) (Table 1). In contrast, the zircon cores from Neoproterozoic ages have high Th/U values of 0.27–1.21 typical of magmatic origin (Table 1). The Late Jurassic–Early Cretaceous zones in zircons are homogenous indicating late-stage recrystallization, while the older Late–Neoproterozoic zircons preserves oscillatory zoning (Figure 6). The oscillatory zoned cores along with high Th/U ratios suggest that the zircons are crystallized from silicate melts, and the obtained ages from these can be considered as crystallization age. There are four rims of Late–Neoproterozoic age which have high Th/U ratio and are discordant. Considering these ages geologically insignificant, we have not considered these points in our weighted mean age calculations. We use the $\pm 3\%$ discordant filter to get the geologically meaningful age. The cluster of data we have considered in age calculation are concordant and is used in weighted mean age calculations.

The zircon grains yielded $^{206}Pb/^{238}U$ ages ranging from ~700 to 846 ($n=29$) Ma with major magmatic pulses between ~700 and 809 Ma ($n=21$) (Figures 6B,C). Fourteen analyses provide an upper intercept age of 776.61 ± 2.72 with a $MSWD = 2.8$ (Figures 6B,C). The sample bears two different ^{206}Pb - ^{238}U age groups; one with weighted mean age of 806.07 ± 1.51 Ma ($MSWD = 1.64$; $n = 6$) which we consider as the zircon crystallization age in the tonalite gneiss whereas another age group with weighted mean age of 782.70 ± 1.43 Ma ($MSWD = 2.68$; $n = 6$; inset of Figure 6D). These two mean ages represent two closely related felsic magmatic pulses at a short time interval.

6 Discussion

6.1 Source characterization and likely tectonic setting of neoproterozoic magmatism in the KT

The studied tonalite gneiss sample is intermediate in composition with $SiO_2=64.85$ wt%, and $MgO=2.88$ wt% and is slightly peraluminous in nature with A/CNK values of 1.1. The high Sr/Y ratio= 19.75 , $La_N/Yb_N=33.99$ ratio point to its similarity with the adakitic rocks (Defant et al., 2002). The Chondrite-normalized spidergram (Figure 5B) shows a

steeply inclined REE pattern (high LREE/HREE ratios) similar to the Neoproterozoic granites of Tibet, and TTG suite (800 Ma) of southern Pamir (e.g., Zhang et al., 2018). The observed features suggest a mafic lower crustal source (e.g., granulite-facies) for the tonalite gneiss. We compared the tonalite gneiss with the granites of similar age from the adjacent terranes of central Tibet to assess their comparative petrogenesis and likely tectonic setting (Table 2; Figure 4). These Neoproterozoic granites are magnesian, calcic to alkali calcic in nature and show affinity with VAG (Figure 4) and follow the calc-alkaline trend (Figure 4). Hence, they bear geochemical features similar to granites formed in the subduction-related tectonic regimes.

6.2 A viable petrogenetic model linking the neoproterozoic magmatism in the KT, Southern Pamir, and Central Tibet

The qualitative analysis of whole-rock elemental data demonstrates that the tonalite gneiss ($SiO_2=64.85$, $MgO=2.88$ wt%, with High LREE/HREE and Sr/Y ratio), might have formed through the melting of a mafic lower crust as noted for the Neoproterozoic TTG suite of the southern Pamir (Zhang et al., 2018), and for fractionated granitoid suite from the Central Tibet (e.g., Amdo and Jiayuqiao) (e.g., Liu et al., 2021). It is therefore imperative to test the hypothesis quantitatively using trace and REE modeling of mafic lower crustal composition (Weaver and Tarney, 1980), which probably formed the Neoproterozoic granitoid of these terranes. In the present study the analyzed sample is from the metamorphic terrane, therefore it is important to decipher the any metamorphic and other alteration effects on the sample. The petrographic features of the tonalite gneiss e.g., 1) primary euhedral crystals of biotite having cleavage in the basal section 2) the absence of sub-solidus deformation in the quartz grains e.g., sub-grain rotation and grain boundary migration etc. suggest that the rock preserved the magmatic texture and has not suffered any alteration and high-grade metamorphism. There are no evidences in this sample for alteration of biotite to chlorite. Any low-grade metamorphism only can affect the alkali element concentrations (e.g., K and Na) and LILE concentrations (e.g., Rb, Ba, Sr, Pb, and Cs). In contrast, these low-grade metamorphic activities have negligible impact on the abundances of immobile elements (e.g., Hu et al., 2018a), therefore, we carried out the REEs modeling in our study.

The melts with a high Sr/Y ratio can be generated at a depth of ~30–40 km (>1.2 GPa) where garnet remains stable with residues of garnet-amphibolite, or eclogite and plagioclase remain unstable (Petford and Gallagher, 2001). The mineral modes ($Gt=0.30$, $Amp=0.10$, $Cpx=0.20$) of a mafic source for

TABLE 2 Compiled Sr-Nd and $\epsilon\text{Hf}(t)$ isotope data from Early-Neoproterozoic magmatic rocks from Northern Lhasa, Qiangtang terrane, Pamir and KT.

	Northern Lhasa (Central Tibet)	Amdo & Jiayuqiao Microcontinent Qiangtang terrane (Central Tibet)	Pamir Plateau	Karakoram Terrane (This Study)
Age (Ma)	856 to ~748	920-767	840-835	800
I_{Sr}	0.708 to 0.711	–	Tonalite, Trondhjemite: 0.705572-0.708341 Granodiorite: 0.700794-701938	–
$\epsilon\text{Nd}(t)$	-2.4 to +10.4	–	Tonalite, Trondhjemite: -9.71 to -8.23 Granodiorite: -4.43 to -5.45	–
$\epsilon\text{Hf}(t)$	-2 to +12.4	-8.9 to +4.0	Tonalite, Trondhjemite: -14 to -10 Granodiorite: -10 to -7	–
Inferences	Derivation from the depleted mantle (juvenile) with the older continental crustal component assimilation (arc and back-arc type)	Protolith derived from partial melting of ancient crustal source	TTG suite derivation from partial melting of a mafic lower crust (≥ 30) km with a garnet amphibolite residue and granodiorite derivation from partial melting of a mafic crust at a shallower level	Derivation from partial melting of a lower crust where garnet remained residue during partial melting
References	Hu et al. (2005); Dong et al. (2011); Hu et al. (2018a); Hu et al. (2018b)	Liu et al. (2021); Guynn et al. (2012); Yu et al. (2021); Zhang et al. (2012)	Zhang et al. (2018)	This Study

TABLE 3 Trace and rare Earth elements (REEs) modeling results for the studied tonalite gneiss (SM 4 M), TTGs of the South Pamir terrane, and Central Tibet.

	Parent (Lower crust, Weaver and Tarney, 1980)	Observed results (SM 4 M (This Study)	Calculated Partial Melting results (F=0.5)	Observed results (Average of TTGs, Zhang et al. (2018), Southern Pamir)	Calculated FC results (F=0.58)(Average of TTGs	Observed results (Average of Granitoids Liu et al. (2021); Yu et al. (2021)Central Tibet)	Calculated FC results (F=0.53)
La	9.5	18.01	18.40	28.12	28.70	30.33	30.90
Ce	17	37.98	31.89	51.67	53.82	64.71	57.42
Pr	2	4.23	3.71	5.80	6.40	6.77	7.00
Nd	8	17.11	13.02	20.91	21.51	23.33	23.38
Sm	2.75	3.67	2.96	4.69	4.86	4.42	5.27
Eu	1.1	0.87	0.98	1.15	1.15	0.71	1.18
Gd	3.95	2.76	2.22	2.86	3.73	4.00	4.06
Tb	0.58	0.38	---	0.35	---	0.62	---
Dy	3.35	1.96	1.59	1.82	2.57	3.85	2.78
Ho	0.73	0.16	---	0.35	---	0.81	---
Er	2	0.45	1.11	0.94	1.86	2.30	2.02
Tm	0.35	0.04	---	0.14	---	0.34	---
Yb	1.9	0.38	0.66	0.90	1.10	2.20	1.20
Lu	0.3	0.06	0.12	0.13	0.20	0.32	0.21

Note: For less fractionated SM, 4 M (SiO₂=64.85, MgO=2.88wt%) the parent is Lower crust (Weaver and Tarney, 1980), while the calculated partial melting results at (F=0.5) were used as the parent for the highly fractionated TTGs (SiO₂=67 wt%; MgO=1.61; Zhang et al., 2018) and Granitoids (SiO₂=71.38 wt%; MgO=1.30; Liu et al., 2021; Yu et al., 2021).

the partial melting model were therefore chosen reasonably at ~900°C and at ~12–15 kbar (Qian and Hermann, 2013). The mineral/liquid partition coefficients (K_d) were taken from Qian and Hermann. (2013), Rollinson. (1993), and from GERM

Partition Coefficient (K_d) Database as given in Supplementary Table S2.

The equilibrium batch melting was performed using the equation (Schilling and Winchester, 1967):

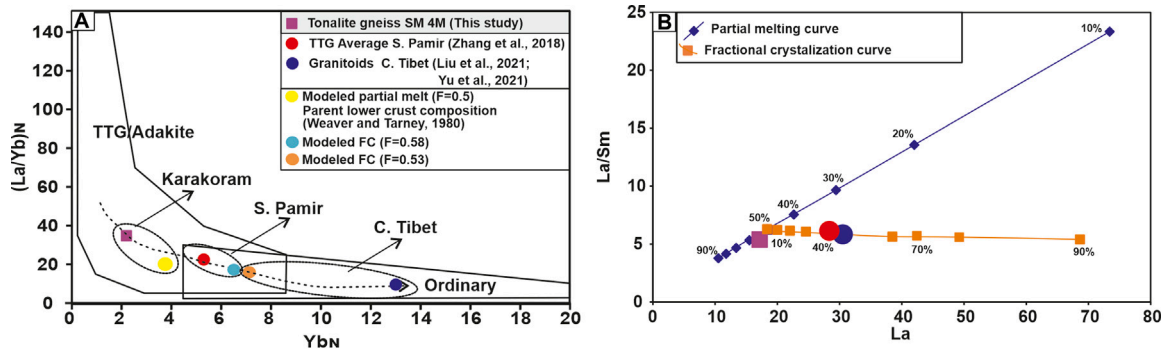


FIGURE 7
 Calculated trends obtained from geochemical modeling of partial melting (PM) of a mafic lower crust (Weaver and Tarney, 1980), and fractional crystallization (FC) of the melt produced (50%) shown in terms of: (A) $(La/Yb)_N$ versus Yb_N (B) La/Sm versus La .

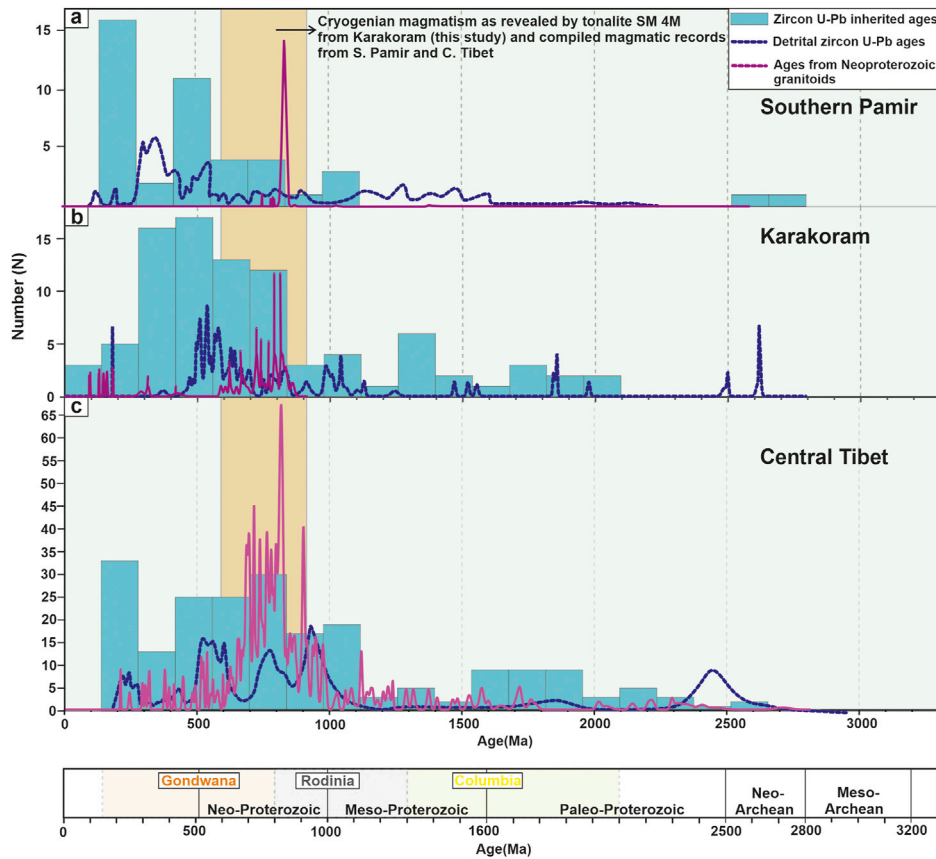


FIGURE 8
 Probability density plot for the inherited zircon ages from the Triassic to Miocene granitoid, U–Pb detrital ages, and Neoproterozoic U–Pb ages from (A) the Karakoram, (B) Southern Pamir, and (C) Central Tibet (Data source-Karakoram: Boutonnet et al., 2012; Fraser et al., 2001; Heuberger et al., 2007; Kumar et al., 2017; Parrish and Tirrul, 1989; Pundir et al., 2020a; Pundir et al., 2020b; Ravikant et al., 2009; Schwab et al., 2004; Searle et al., 1998; Sen et al., 2014; Van buer et al., 2015; Weinberg et al., 2000; Southern Pamir: Chapman et al., 2018; Liu et al., 2020; Schwab et al., 2004; Central Tibet: Hao et al., 2016; Ou et al., 2017; Schwab et al., 2004; Sui et al., 2013; Wang et al., 2020; Wu et al., 2016; Zhai et al., 2013). Density plots of U–Pb detrital ages are taken from previous studies. Tibet: Gehrels et al., 2011; He et al., 2019; Song et al., 2017; Pamir: Chapman et al., 2018; Karakoram: Borneman et al., 2015. Density plots of Neoproterozoic U–Pb ages. Data Source: Tibet: Hu et al., 2005; Dong et al., 2011; Liu et al., 2021; Yu et al., 2021 (n=290), Karakoram: This study (n=45), Pamir: Zhang et al., 2018 (n=199).

$$\frac{C_L}{C_0} = \frac{1}{F + D - FD} \quad (1)$$

where, C_L and C_0 are the concentrations of an element in the melt and source respectively, F is the weight fraction of melt, and D is the bulk distribution coefficient.

For fractional crystallization we used the Rayleigh fractionation equation (Rayleigh, 1896):

$$\frac{C_L}{C_0} = F^{D-1} \quad (2)$$

where, C_L and C_0 are the concentrations of an element in the residual melt and parent magma respectively, F is the weight fraction of residual melt, and D is the bulk distribution coefficient. We consider the proportions (Bt=0.20, Plg=0.45, Kfs=0.05, Qz=0.30) of mineral mode present in the studied tonalite gneiss as fractionating phases.

The calculated results are summarized in Table 3 and trends of partial melting and fractional crystallization are shown on (La/Yb)_N vs. Yb_N (Martin, 1986) (Figure 7A) on La/Sm vs. La (Figure 7B). The calculated results suggest that about 50% melting of a mafic lower crustal source can generate a composition similar to the tonalite gneiss SM 4 M (SiO₂=64.85, MgO=2.88wt%). Further fractional crystallization (FC) (~42%) of generated melt can produce rock members similar to the Tonalite-trondhjemite suite (SiO₂=67 wt%; MgO=1.61; average of Zhang et al., 2018 geochemical data) from the Southern Pamir, and about 47% FC can produce rock members similar to the granitoid suite (SiO₂=71.4 wt%; MgO=1.3; average of Liu et al., 2021; Yu et al., 2021) from the Central Tibet (Table 3). The generation of the SM 4 M at a high degree of partial melting (40%–60%) also supports its affinity toward the tonalitic nature of the melt (Arndt, 2013). It is therefore likely that melt similar to the low SiO₂ and high MgO tonalite gneiss SM 4 M served as parental magma which evolved through fractional differentiation forming the high SiO₂ and low MgO rock members of the TTG suites of southern Pamir and granitoid from Central Tibet. Based on geochemical and zircon Lu-Hf isotope data Liu et al., 2021 also suggested that the granodiorites and tonalites as the protolith of the central Tibet granitic gneisses. However, the likely genetic connotation between KT tonalite gneiss and rocks of TTG from Pamir needs to be tested further using a large database.

6.3 Pamir-karakoram-Tibet as fragments of rodinia supercontinent

We compile zircon U-Pb inherited ages from the Triassic to Miocene granitoid and detrital zircon U-Pb geochronological records from southern Pamir, Karakoram, and central Tibet, and compare them with Neoproterozoic magmatism of these terranes to decipher the geological

magmatic history of these blocks during the Rodinia supercontinent cycle (Figure 8). The data compilation suggests that the terranes witnessed intense magmatism during Neoproterozoic and Cambrian times (Figure 8). We also compile the Sr-Nd and zircon Lu-Hf isotope values of the granitoids of ~920–748 Ma from these terranes to assess their comparative petrogenesis and the likely source of their formation (Table 2). The negative to positive εNd_(t) and εHf_(t) isotope values from the Early-Middle Neoproterozoic sedimentary deposits, as well as bedrock granite gneisses from Tibet along with high (⁸⁷Sr/⁸⁶Sr)_i values of 0.708–0.711 (Table 2), suggest the origin of the granitoids from depleted mantle with the older continental crustal component assimilation (Table 2; Yu et al., 2021). However, the Neoproterozoic (857–767 Ma) granite gneiss from the Amdo & Jiayuqiao microcontinents from the Qiangtang terrane, Central Tibet have highly negative to positive values (–8.9 to 4.0), and geochemically the granite gneiss bears calc-alkaline nature, with the protolith derived from partial melting of ancient crustal source (e.g., tonalites and granodiorites) (Table 2; Liu et al., 2021). Similarly, the middle Neoproterozoic (~840 Ma) TTG suite from the central Pamir also have εNd_(i) (–14 to –10) and zircon εHf_(i) (–9.5 to –8.7) and geochemically the granitoids belong to TTG/adakites suites having enriched LILE, and LREEs as compared to HFSEs and HREEs with high Sr/Y and (La/Yb)_N ratios suggesting its origin from partial melting of a mafic lower crust (Zhang et al., 2018). Our observed geochemical results from the present study also suggest that the tonalite gneiss (SM 4 M) from the eastern Karakoram melt might have derived from partial melting of the mafic lower continental crust (Figure 5B). Therefore, we argue that these continents might have experienced a similar geotectonic evolution during Neoproterozoic time. Considering limitations of interpretation based on only one sample of tonalite gneiss, it cannot be argued firmly the exact position of the KT within the Rodinia supercontinent but the theory of plate tectonics suggests that no rock is accidental (Fichter and Whitmeyer, 2019). The reason we got only one tonalite sample of Cryogenian age in this zone might be that partial migmatization have annealed and recrystallized the zircons of the Late Neo-Proterozoic terrane. Therefore, we argue that this sample bears significance in the Rodinia supercontinent reconstruction. Based on identical geochemical and geochronological records from the Karakoram and south-central Pamir, we propose the Karakoram, south-central Pamir and central Tibet microcontinents as a single continental block during Neoproterozoic. The Late Jurassic-Early Cretaceous rims from the zircons are homogenous indicating the tonalite gneiss have recorded thermal imprints during the subduction of Neo-Tethys Oceanic lithosphere along the Eurasian Plate margin.

7 Conclusions

The elemental data suggest that the studied tonalite gneiss is more likely sourced from the mafic lower crust where garnet remained in the residue. Petrogenetic modeling suggests that the parental melt similar to the tonalite gneiss can be generated by ~50% partial melting of the mafic lower crust which might have served as the parent to the TTGs and the more evolved granitoid suite from the Southern Pamir and Central Tibet during Neoproterozoic. The middle-Neoproterozoic tonalite gneiss, recorded for the first time from the KT, suggests Karakoram, south-central Pamir and central Tibet microcontinents as a single continental block during Neoproterozoic.

Data availability statement

The original contributions presented in the study are included in the article/[Supplementary Material](#), further inquiries can be directed to the corresponding author.

Author contributions

SP wrote the manuscript with inputs from VA and SK. VA acquired funding for the research and did project administration. SS and SD produced the zircon U-Pb geochronological results.

Funding

This work was supported by Science and Engineering Research Board grant EMR/2014/000555 and Activity 7 of the WIHG CAP Himalaya awarded to VA.

References

- Arndt, N. T. (2013). Formation and evolution of the continental crust. *Geochem. Perspect.* 2 (3), 405–533. doi:10.7185/geochempersp.2.3
- Borneman, N. L., Hodges, K. V., Van Soest, M. C., Bohon, W., Wartho, J. A., Cronk, S. S., et al. (2015). Age and structure of the Shyok suture in the Ladakh region of northwestern India: Implications for slip on the Karakoram fault system. *Tectonics* 34 (10), 2011–2033. doi:10.1002/2015TC003933
- Bose, S., Adlaka, V., and Pundir, S. (2022). Submagmatic flow to solid-state ductile deformation of the Karakoram Batholith, India: Insights into syn-tectonic cooling and exhumation. *Int. J. Earth Sci.* 1–16, 2337–2352. doi:10.1007/s00531-022-02236-8
- Boutonnet, E., Leloup, P. H., Arnaud, N., Paquette, J. L., Davis, W. J., and Hattori, K. (2012). Synkinematic magmatism, heterogeneous deformation, and progressive strain localization in a strike-slip shear zone: The case of the right-lateral Karakoram fault. *Tectonics* 31 (4), 3049. doi:10.1029/2011TC003049
- Cawood, P. A., Strachan, R. A., Pisarevsky, S. A., Gladkochub, D. P., and Murphy, J. B. (2016). Linking collisional and accretionary orogens during Rodinia assembly and breakup: Implications for models of supercontinent cycles. *Earth Planet. Sci. Lett.* 449, 118–126. doi:10.1016/j.epsl.2016.05.049
- Cawood, P. A., Wang, Y., Xu, Y., and Zhao, G. (2013). Locating South China in Rodinia and Gondwana: A fragment of greater India lithosphere? *Geology* 41 (8), 903–906. doi:10.1130/G34395.1
- Chapman, J. B., Scoggin, S. H., Kapp, P., Carrapa, B., Ducea, M. N., Worthington, J., et al. (2018). Mesozoic to Cenozoic magmatic history of the Pamir. *Earth Planet. Sci. Lett.* 482, 181–192. doi:10.1016/j.epsl.2017.10.041
- Condie, K. C. (2001). Continental growth during formation of Rodinia at 1.35–0.9 Ga. *Gondwana Res.* 4, 5–16. doi:10.1016/s1342-937x(05)70650-x
- Crawford, A. R. (1974). The Indus suture line, the Himalaya, Tibet and Gondwanaland. *Geol. Mag.* 111 (5), 369–383. doi:10.1017/S0016756800039935
- Dan, W., Wang, Q., Zhang, X. Z., and Tang, G. J. (2020). Early Paleozoic S-type granites as the basement of southern Qiantang terrane, Tibet. *Lithos* 356, 105395. doi:10.1016/j.lithos.2020.105395
- Defant, M. J., Xu, J. F., Kepezhinskas, P., Wang, Q., Zhang, Q., and Xiao, L. (2002). Adakites: Some variations on a theme. *Acta Pet. Sin.* 18, 129–142.
- Dong, X., Zhang, Z., Santosh, M., Wang, W., Yu, F., and Liu, F. (2011). Late Neoproterozoic thermal events in the northern Lhasa terrane, south Tibet: Zircon

Acknowledgments

Director, Wadia Institute of Himalayan Geology, Dehradun, is thanked for motivation and generous support during the research work. Manoranjan Mohanty and Rajwant, Department of Science and Technology (DST) and Science and Engineering Research Board (SERB), New Delhi, are thanked for their continuous support and encouragement. Naresh Kumar Juyal helped during CL imaging, and Chandra Shekhar helped while ICPMS and XRF analyses. Chhutapa Phuntsog Dorjay, Skalzang Namgyal, and Thinless Gyachho are thanked for field assistance. The Indo-Tibetan Border Police is highly acknowledged for help during fieldwork in Ladakh, NW India.

Conflict of interest

The authors declare that the research was conducted in the absence of any commercial or financial relationships that could be construed as a potential conflict of interest.

Publisher's note

All claims expressed in this article are solely those of the authors and do not necessarily represent those of their affiliated organizations, or those of the publisher, the editors and the reviewers. Any product that may be evaluated in this article, or claim that may be made by its manufacturer, is not guaranteed or endorsed by the publisher.

Supplementary material

The Supplementary Material for this article can be found online at: <https://www.frontiersin.org/articles/10.3389/feart.2022.1027801/full#supplementary-material>

- chronology and tectonic implications. *J. Geodyn.* 52 (5), 389–405. doi:10.1016/j.jog.2011.05.002
- Fichter, L. S., and Whitmeyer, S. J. (2019). No rock is accidental! Stratigraphy, structure, and tectonics in the Wilson cycle. *Dev. Struct. Geol. Tect.* 5, 145–160. doi:10.1016/b978-0-12-814048-2.00012-0
- Fort, P. L., Tongiorgi, M., and Gaetani, M. (1994). Discovery of a crystalline basement and Early Ordovician marine transgression in the Karakorum mountain range, Pakistan. *Geol.* 22 (10), 941–944. doi:10.1130/0091-7613(1994)022<0941:doacba>2.3.co;2
- Fraser, J. E., Searle, M. P., Parrish, R. R., and Noble, S. R. (2001). Chronology of deformation, metamorphism, and magmatism in the southern Karakoram Mountains. *Geol. Soc. Am. Bull.* 113 (11), 1443–1455. doi:10.1130/0016-7606(2001)113<1443:codmam>2.0.co;2
- Frost, B. R., Barnes, C. G., Collins, W. J., Arculus, R. J., Ellis, D. J., and Frost, C. D. (2001). A geochemical classification for granitic rocks. *J. Petrology* 42 (11), 2033–2048. doi:10.1093/petrology/42.11.2033
- Gehrels, G., Kapp, P., DeCelles, P., Pullen, A., Blakey, R., Weislogel, A., et al. (2011). Detrital zircon geochronology of pre-Tertiary strata in the Tibetan-Himalayan orogen. *Tectonics* 30 (5). doi:10.1029/2011TC002868
- Guyon, J., Kapp, P., Gehrels, G. E., and Ding, L. (2012). U–Pb geochronology of basement rocks in central Tibet and paleogeographic implications. *J. Asian Earth Sci.* 43 (1), 23–50. doi:10.1016/j.jseae.2011.09.003
- Hao, L. L., Wang, Q., Wyman, D. A., Ou, Q., Dan, W., Jiang, Z. Q., et al. (2016). Underplating of basaltic magmas and crustal growth in a continental arc: Evidence from Late Mesozoic intermediate–felsic intrusive rocks in southern Qiangtang, central Tibet. *Lithos* 245, 223–242. doi:10.1016/j.lithos.2015.09.015
- He, J., Kapp, P., Chapman, J. B., DeCelles, P. G., and Carrapa, B. (2019). A history of the Asian monsoon and its interactions with solid Earth tectonics in Cenozoic South Asia. *Geol. Soc. Spec. Publ.* 483 (1), 631–652. doi:10.1144/SP483.1
- Heuberger, S., Schaltegger, U., Burg, J. P., Villa, I. M., Frank, M., Dawood, H., et al. (2007). Age and isotopic constraints on magmatism along the Karakoram–Kohistan suture zone, NW Pakistan: Evidence for subduction and continued convergence after India–Asia collision. *Swiss J. Geosci.* 100 (1), 85–107. doi:10.1007/s00015-007-1203-7
- Hu, D., Wu, Z., Jiang, W., Shi, Y., Ye, P., and Liu, Q. (2005). SHRIMP zircon U–Pb age and Nd isotopic study on the Nyainqentanglha Group in Tibet. *Sci. China Ser. D-Earth. Sci.* 48 (9), 1377–1386. doi:10.1360/04yd0183
- Hu, P. Y., Zhai, Q. G., Wang, J., Tang, Y., Wang, H. T., and Hou, K. J. (2018a). Precambrian origin of the north Lhasa terrane, Tibetan plateau: Constraint from early cryogenian back-arc magmatism. *Precambrian Res.* 313, 51–67. doi:10.1016/j.precamres.2018.05.014
- Hu, P. Y., Zhai, Q. G., Wang, J., Tang, Y., Wang, H. T., Zhu, Z. C., et al. (2018b). Middle Neoproterozoic (ca. 760 Ma) arc and back-arc system in the North Lhasa terrane, Tibet, inferred from coeval N–MORB and arc-type gabbros. *Precambrian Res.* 316, 275–290. doi:10.1016/j.precamres.2018.08.022
- Jain, A. K., and Singh, S. (2009). *Geology and tectonics of the southeastern Ladakh and Karakoram*. Bangalore: Geological society of India City.
- Jain, A. K., and Singh, S. (2008). Tectonics of the southern Asian Plate margin along the Karakoram shear zone: Constraints from field observations and U–Pb SHRIMP ages. *Tectonophysics* 451 (1–4), 186–205. doi:10.1016/j.tecto.2007.11.048
- Jain, A. K. (2014). When did India–Asia collide and make the Himalaya? *Curr. Sci.* 106 (2), 254–266.
- Janoušek, V., Farrow, C. M., and Erban, V. (2006). Interpretation of whole-rock geochemical data in igneous geochemistry: Introducing geochemical data Toolkit (GCDkit). *J. Pet.* 47 (6), 1255–1259. doi:10.1093/petrology/egl013
- Kang, H., Li, D., Chen, Y., Song, L., Xue, G., Geng, J., et al. (2019). Micro-continental blocks in Gondwana assembly: Geological and geochemical evidence of the Indochina block, SE Tibetan Plateau. *Lithos* 326, 460–475. doi:10.1016/j.lithos.2019.01.002
- Kapp, P., Murphy, M. A., Yin, A., Harrison, T. M., Ding, L., and Guo, J. (2003). Mesozoic and Cenozoic tectonic evolution of the Shiquanhe area of Western Tibet. *Tectonics* 22 (4), 1332. doi:10.1029/2001tc001332
- Khanna, P. P. (2009). An appraisal of ICP–ms technique for determination of REEs: Long term QC assessment of silicate rock analysis. *Him. Geol.* 30, 95–99.
- Kumar, S., Bora, S., Sharma, U. K., Yi, K., and Kim, N. (2017). Early Cretaceous subvolcanic calc-alkaline granitoid magmatism in the Nubra–Shyok valley of the Shyok suture zone, Ladakh Himalaya, India: Evidence from geochemistry and U–Pb SHRIMP zircon geochronology. *Lithos* 277, 33–50. doi:10.1016/j.lithos.2016.11.019
- Le Maitre, R. W. (2002). *A classification of igneous rocks: A classification and glossary of terms: Recommendations of the international union of geological sciences subcommission of the systematic of igneous rocks*. Cambridge, New York, Melbourne, VIC: Cambridge University Press.
- Li, Z. X., Bogdanova, S., Collins, A. S., Davidson, A., De Waele, B., Ernst, R. E., et al. (2008). Assembly, configuration, and break-up history of Rodinia: A synthesis. *Precambrian Res.* 160 (1–2), 179–210. doi:10.1016/j.precamres.2007.04.021
- Liu, X. Q., Zhang, C. L., Hao, X. S., Zou, H., Zhao, H. X., and Ye, X. T. (2020). Early Cretaceous granitoids in the southern Pamir: Implications for the meso-tethys evolution of the Pamir plateau. *Lithos* 362, 105492. doi:10.1016/j.lithos.2020.105492
- Liu, Y., Wang, Y., Li, S., Santosh, M., Guo, R., and Yu, S. (2021). Neoproterozoic Amdo and Jiayuqiao microblocks in the Tibetan plateau: Implications for Rodinia reconstruction. *Bulletin* 133 (3–4), 663–678. doi:10.1130/B35632.1
- Martin, H. (1986). Effect of steeper Archean geothermal gradient on geochemistry of subduction-zone magmas. *Geol.* 14 (9), 753–756. doi:10.1130/0091-7613(1986)14<753:eosagg>2.0.co;2
- Meert, J. G., and Torsvik, T. H. (2003). The making and unmaking of a supercontinent: Rodinia revisited. *Tectonophysics* 375 (1–4), 261–288. doi:10.1016/s0040-1951(03)00342-1
- Merdith, A. S., Williams, S. E., Müller, R. D., and Collins, A. S. (2017). Kinematic constraints on the Rodinia to Gondwana transition. *Precambrian Res.* 299, 132–150. doi:10.1016/j.precamres.2017.07.013
- Mukherjee, P. K., Singhal, S., Adlakha, V., Rai, S. K., Dutt, S., Kharya, A., et al. (2017). *In situ* U–Pb zircon micro-geochronology of MCT zone rocks in the lesser Himalaya using LA–MC–ICPMS technique. *Curr. Sci.* 112, 802–810. doi:10.18520/cs/v112/i04/802-810
- Ou, Q., Wang, Q., Wyman, D. A., Zhang, H. X., Yang, J. H., Zeng, J. P., et al. (2017). Eocene adakitic porphyries in the central-northern Qiangtang Block, central Tibet: Partial melting of thickened lower crust and implications for initial surface uplifting of the plateau. *J. Geophys. Res. Solid Earth* 122 (2), 1025–1053. doi:10.1002/2016JB013259
- Parrish, R. R., and Tirrul, R. (1989). U–Pb age of the Baltoro granite, northwest Himalaya, and implications for monazite U–Pb systematics. *Geol.* 17 (12), 1076–1079. doi:10.1130/0091-7613(1989)017<1076:upaotb>2.3.co;2
- Paton, C., Hellstrom, J., Paul, B., Woodhead, J., and Hergt, J. (2011). Iolite: Freeware for the visualisation and processing of mass spectrometric data. *J. Anal. At. Spectrom.* 26 (12), 2508–2518. doi:10.1039/C1JA10172B
- Pearce, J. A., Harris, N. B., and Tindle, A. G. (1984). Trace element discrimination diagrams for the tectonic interpretation of granitic rocks. *J. Petrology* 25 (4), 956–983. doi:10.1093/petrology/25.4.956
- Peng, T., Zhao, G., Fan, W., Peng, B., and Mao, Y. (2015). Late Triassic granitic magmatism in the eastern Qiangtang, eastern Tibetan plateau: Geochronology, petrogenesis and implications for the tectonic evolution of the paleo-tethys. *Gondwana Res.* 27 (4), 1494–1508. doi:10.1016/j.gr.2014.01.009
- Petford, N., and Gallagher, K. (2001). Partial melting of mafic (amphibolitic) lower crust by periodic influx of basaltic magma. *Earth Planet. Sci. Lett.* 193 (3–4), 483–499. doi:10.1016/s0012-821x(01)00481-2
- Phillips, R. J., Searle, M. P., and Parrish, R. R. (2013). The geochemical and temporal evolution of the continental lithosphere and its relationship to continental-scale faulting: The Karakoram Fault, eastern Karakoram, NW Himalayas. *Geochem. Geophys. Geosyst.* 14 (3), 583–603. doi:10.1002/ggge.20061
- Pundir, S., Adlakha, V., Kumar, S., and Singhal, S. (2020a). Closure of India–Asia collision margin along the Shyok suture zone in the eastern Karakoram: New geochemical and zircon U–Pb geochronology observations. *Geol. Mag.* 157 (9), 1451–1472. doi:10.1017/S0016756819001547
- Pundir, S., Adlakha, V., Kumar, S., Singhal, S., and Sen, K. (2020b). Petrology, geochemistry and geochronology of granites and granite gneisses in the SE Karakoram, India: Record of subduction-related and pre-to syn-kinematic magmatism in the Karakoram Fault zone. *Mineral. Pet.* 114 (5), 413–434. doi:10.1007/s00710-020-00706-y
- Qian, Q., and Hermann, J. (2013). Partial melting of lower crust at 10–15 kbar: Constraints on adakite and TTG formation. *Contrib. Mineral. Pet.* 165 (6), 1195–1224. doi:10.1007/s00410-013-0854-9
- Ravikant, V., Wu, F. Y., and Ji, W. Q. (2009). Zircon U–Pb and Hf isotopic constraints on petrogenesis of the Cretaceous–Tertiary granites in eastern Karakoram and Ladakh, India. *Lithos* 110 (1–4), 153–166. doi:10.1016/j.lithos.2008.12.013
- Rayleigh, L. (1896). *Theoretical considerations respecting the separation of gases by diffusion and similar processes*. Lond. Edinb. Dublin Philosophical Mag. J. Sci. 42 (259), 493–498. doi:10.1080/14786449608620944
- Reichardt, H., Weinberg, R. F., Andersson, U. B., and Fanning, C. M. (2010). Hybridization of granitic magmas in the source: The origin of the Karakoram Batholith, Ladakh, NW India. *Lithos* 116 (3–4), 249–272. doi:10.1016/j.lithos.2009.11.013
- Robinson, A. C. (2015). Mesozoic tectonics of the Gondwanan terranes of the Pamir plateau. *J. Asian Earth Sci.* 102, 170–179. doi:10.1016/j.jseae.2014.09.012

- Rolland, Y., Mahéo, G., Pècher, A., and Villa, I. M. (2009). Syn-kinematic emplacement of the Pangong metamorphic and magmatic complex along the Karakoram fault (N Ladakh). *J. Asian Earth Sci.* 34 (1), 10–25. doi:10.1016/j.jseas.2008.03.009
- Rolland, Y., Picard, C., Pècher, A., Carrio, E., Sheppard, S. M., Oddone, M., et al. (2002). Presence and geodynamic significance of Cambro-Ordovician series of SE Karakoram (N Pakistan). *Geodin. Acta* 15 (1), 1–21. doi:10.1080/09853111.2002.10510736
- Rollinson, H. (1993). Using geochemical data. *Eval. Present. Interpret.* 1993, 1.
- Rubatto, D. (2002). Zircon trace element geochemistry: Partitioning with garnet and the link between U–Pb ages and metamorphism. *Chem. Geol.* 184 (1–2), 123–138. doi:10.1016/S0009-2541(01)00355-2
- Saini, N. K., Mukherjee, P. K., Khanna, P. P., and Purohit, K. K. (2007). A proposed amphibolite reference rock sample (AM-H) from Himachal Pradesh. *J. Geol. Soc. India* 69 (4), 799.
- Schilling, J. G., and Winchester, J. W. (1967). “Rare-Earth fractionation and magmatic processes,” in *Mantles of earth and terrestrial planets*. Editor S. K. Runcorn (New York: Interscience), 267–283.
- Schwab, M., Ratschbacher, L., Siebel, W., McWilliams, M., Minaev, V., Lutkov, V., et al. (2004). Assembly of the Pamirs: Age and origin of magmatic belts from the southern Tien Shan to the southern Pamirs and their relation to Tibet. *Tectonics* 23 (4), 1583. doi:10.1029/2003tc001583
- Searle, M. P. (2011). Geological evolution of the Karakoram ranges. *Ital. J. Geosci.* 130 (2), 147–159. doi:10.3301/IJG.2011.08
- Searle, M. P., and Hacker, B. R. (2019). Structural and metamorphic evolution of the Karakoram and Pamir following India–Kohistan–Asia collision. *Geol. Soc. Spec. Publ.* 483 (1), 555–582. doi:10.1144/sp483.6
- Searle, M. P., Weinberg, R. F., and Dunlap, W. J. (1998). Transpressional tectonics along the Karakoram Fault zone, northern Ladakh: Constraints on Tibetan extrusion. *Geol. Soc. Spec. Publ.* 135 (1), 307–326. doi:10.1144/gsl.sp.1998.135.01.20
- Sen, K., Mukherjee, B. K., and Collins, A. S. (2014). Interplay of deformation and magmatism in the Pangong Transpression Zone, eastern Ladakh, India: Implications for remobilization of the trans-Himalayan magmatic arc and initiation of the Karakoram Fault. *J. Struct. Geol.* 62, 13–24. doi:10.1016/j.jsg.2014.01.009
- Sengör, A. C. (1984). The Cimmeride orogenic system and the tectonics of Eurasia. *Geol. Soc. Am. Spec. Pap.* 195, 82.
- Sláma, J., Košler, J., Condon, D. J., Crowley, J. L., Gerdes, A., Hanchar, J. M., et al. (2008). Plešovice zircon—A new natural reference material for U–Pb and Hf isotopic microanalysis. *Chem. Geol.* 249 (1–2), 1–35. doi:10.1016/j.chemgeo.2007.11.005
- Song, P., Ding, L., Li, Z., Lippert, P. C., and Yue, Y. (2017). An early bird from Gondwana: Paleomagnetism of lower permian lavas from northern Qiangtang (Tibet) and the geography of the paleo-tethys. *Earth Planet. Sci. Lett.* 475, 119–133. doi:10.1016/j.epsl.2017.07.023
- Srimal, N. (1986). India-Asia collision: Implications from the geology of the eastern Karakoram. *Geol.* 14 (6), 523–527. doi:10.1130/0091-7613(1986)14<523:iciftg>2.0.co;2
- Strecheisen, A. (1976). To each plutonic rock its proper name. *Earth-science Rev.* 12 (1), 1–33. doi:10.1016/0012-8252(76)90052-0
- Streule, M. J., Phillips, R. J., Searle, M. P., Waters, D. J., and Horstwood, M. S. A. (2009). Evolution and chronology of the Pangong metamorphic complex adjacent to the Karakoram Fault, Ladakh: Constraints from thermobarometry, metamorphic modelling and U–Pb geochronology. *J. Geol. Soc. Lond.* 166 (5), 919–932. doi:10.1144/0016-76492008-117
- Sui, Q. L., Wang, Q., Zhu, D. C., Zhao, Z. D., Chen, Y., Santosh, M., et al. (2013). Compositional diversity of ca. 110 Ma magmatism in the northern Lhasa terrane, Tibet: Implications for the magmatic origin and crustal growth in a continent–continent collision zone. *Lithos* 168, 144–159. doi:10.1016/j.lithos.2013.01.012
- Sun, S. S., and McDonough, W. F. (1989). Chemical and isotopic systematics of oceanic basalts: Implications for mantle composition and processes. *Geol. Soc. Spec. Publ.* 42 (1), 313–345. doi:10.1144/GSL.SP.1989.042.01.19
- Van Buer, N. J., Jagoutz, O., Upadhyay, R., and Guillong, M. (2015). Mid-crustal detachment beneath Western Tibet exhumed where conjugate Karakoram and Longmu–Gozha Co faults intersect. *Earth Planet. Sci. Lett.* 413, 144–157. doi:10.1016/j.epsl.2014.12.053
- Vermeesch, P. (2018). IsoplotR: A free and open toolbox for geochronology. *Geosci. Front.* 9 (5), 1479–1493. doi:10.1016/j.gsf.2018.04.001
- Villarreal, D. P., Robinson, A. C., Carrapa, B., Worthington, J., Chapman, J. B., Oimahmadov, I., et al. (2020). Evidence for late triassic crustal suturing of the central and southern Pamir. *J. Asian Earth Sci.* X 3, 100024. doi:10.1016/j.jaesx.2019.100024
- Wallis, D., Phillips, R. J., and Lloyd, G. E. (2014). Evolution of the eastern Karakoram metamorphic complex, Ladakh, NW India, and its relationship to magmatism and regional tectonics. *Tectonophysics* 626, 41–52. doi:10.1016/j.tecto.2014.03.023
- Wang, H., Zhai, Q., Hu, P., Zeng, L., Tang, Y., and Zhu, Z. (2020). Early paleozoic granitic rocks of the South Qiangtang terrane, northern Tibetan plateau: Implications for subduction of the proto-(paleo)-tethys ocean. *J. Asian Earth Sci.* 204, 104579. doi:10.1016/j.jseas.2020.104579
- Weaver, B. L., and Tarney, J. (1980). Continental crust composition and nature of the lower crust: Constraints from mantle Nd–Sr isotope correlation. *Nature* 286 (5771), 342–346. doi:10.1038/286342a0
- Weinberg, R. F., Dunlap, W. J., and Whitehouse, M. (2000). New field, structural and geochronological data from the Shyok and nubra valleys, northern Ladakh: Linking Kohistan to Tibet. *Geol. Soc. Spec. Publ.* 170 (1), 253–275. doi:10.1144/gsl.sp.2000.170.01.14
- Weinberg, R. F., and Mark, G. (2008). Magma migration, folding, and disaggregation of migmatites in the Karakoram shear zone, Ladakh, NW India. *Geol. Soc. Am. Bull.* 120 (7–8), 994–1009. doi:10.1130/b26227.1
- Whitney, D. L., and Evans, B. W. (2010). Abbreviations for names of rock-forming minerals. *Am. Mineral.* 95 (1), 185–187. doi:10.2138/am.2010.3371
- Wiedenbeck, M. A. P. C., Alle, P., Corfu, F. Y., Griffin, W. L., Meier, M., Oberli, F. V., et al. (1995). Three natural zircon standards for U–Th–Pb, Lu–Hf, trace element and REE analyses. *Geostand. Geanal. Res.* 19 (1), 1–23. doi:10.1111/j.1751-908x.1995.tb00147.x
- Wu, H., Xie, C., Li, C., Wang, M., Fan, J., and Xu, W. (2016). Tectonic shortening and crustal thickening in subduction zones: Evidence from middle–late jurassic magmatism in southern Qiangtang, China. *Gondwana Res.* 39, 1–13. doi:10.1016/j.gr.2016.06.009
- Yeh, M. W., and Shellnutt, J. G. (2016). The initial break-up of Pangaea elicited by Late Paleozoic deglaciation. *Sci. Rep.* 6 (1), 31442–31449. doi:10.1038/srep31442
- Yu, Y. P., Xie, C. M., Dong, Y. S., Dong, Y. C., Wang, B., Duan, M. L., et al. (2021). Early Neoproterozoic granitic gneisses in the Amdo micro-continent, Tibet: Petrogenesis and geodynamic implications. *Int. Geol. Rev.* 63 (3), 342–356. doi:10.1080/00206814.2019.1710866
- Zhai, Q. G., Jahn, B. M., Su, L., Wang, J., Mo, X. X., Lee, H. Y., et al. (2013). Triassic arc magmatism in the Qiangtang area, northern Tibet: Zircon U–Pb ages, geochemical and Sr–Nd–Hf isotopic characteristics, and tectonic implications. *J. Asian Earth Sci.* 63, 162–178. doi:10.1016/j.jseas.2012.08.025
- Zhang, C. L., Zou, H. B., Ye, X. T., and Chen, X. Y. (2018). A newly identified Precambrian terrane at the Pamir Plateau: The Archean basement and Neoproterozoic granitic intrusions. *Precambrian Res.* 304, 73–87. doi:10.1016/j.precamres.2017.11.006
- Zhang, Z. M., Dong, X., Liu, F., Lin, Y. H., Yan, R., and Santosh, M. (2012). Tectonic evolution of the Amdo terrane, central Tibet: Petrochemistry and zircon U–Pb geochronology. *J. Geol.* 120 (4), 431–451. doi:10.1086/665799
- Zhao, G., Wang, Y., Huang, B., Dong, Y., Li, S., Zhang, G., et al. (2018). Geological reconstructions of the east Asian blocks: From the breakup of Rodinia to the assembly of pangea. *Earth. Sci. Rev.* 186, 262–286. doi:10.1016/j.earscirev.2018.10.003
- Zhou, X., Zheng, J., Li, Y., Griffin, W. L., Xiong, Q., Moghadam, H. S., et al. (2019). Neoproterozoic sedimentary rocks track the location of the Lhasa Block during the Rodinia breakup. *Precambrian Res.* 320, 63–77. doi:10.1016/j.precamres.2018.10.005